



1 **Chlorine oxidation of VOCs at a semi-rural site in Beijing: Significant**
2 **chlorine liberation from ClNO₂ and subsequent gas and particle phase Cl-**
3 **VOC production**

4 Michael Le Breton¹, Åsa M Hallquist², Ravi Kant Pathak¹, David Simpson^{3,4}, Yujue Wang⁵,
5 John Johansson³, Jing Zheng⁵, Yudong Yang⁵, Dongjie Shang⁵, Haichao Wang⁵, Qianyun Liu⁶,
6 Chak Chan⁷, Tao Wang⁸, Thomas J. Bannan⁹, Michael Priestley⁹, Carl J Percival^{9*}, Dudley E
7 Shallcross¹⁰, Keding Lu⁵, Song Guo⁵, Min Hu⁵ and Mattias Hallquist¹

8 ¹Department of Chemistry and Molecular Biology, University of Gothenburg, Gothenburg, Sweden

9 ²IVL Swedish Environmental Research Institute, Gothenburg, Sweden

10 ³Earth and Space Sciences, Chalmers University of Technology, Gothenburg, Sweden

11 ⁴Norwegian Meteorological Institute, Oslo, Norway

12 ⁵State Key Joint Laboratory of Environmental Simulation and Pollution Control, College of Environmental
13 Sciences and Engineering, Peking University, Beijing, China

14 ⁶Division of Environment and Sustainability, The Hong Kong University of Science and Technology, Clearwater
15 Bay, Kowloon, Hong Kong

16 ⁷School of Energy and Environment, City University of Hong Kong, Hong Kong

17 ⁸Department of Civil and Environmental Engineering, The Hong Kong Polytechnic University, Hong Kong, China

18 ⁹Centre for Atmospheric Science, School of Earth, Atmospheric and Environmental Science, University of
19 Manchester, Manchester, UK

20 ¹⁰School of Chemistry, University of Bristol, Cantock's Close, Bristol, BS8 1TS, UK

21 * Now at Jet Propulsion laboratory, Pasadena, California, USA.

22
23 Correspondence to: M. le Breton (Michael.le.breton@gu.se)

24

25 **Abstract.** Nitryl Chloride (ClNO₂) accumulation at night-time acts as a significant reservoir for active chlorine
26 and impacts the following day's photochemistry when the chlorine atom is liberated at sunrise. Here, we report
27 simultaneous measurements of N₂O₅, a suite of inorganic halogens including ClNO₂ and Cl-VOCs in the gas and
28 particle phase utilizing the FIGAERO-ToF-CIMS during an intensive measurement campaign 40 km Northwest
29 of Beijing in May and June 2016. A maximum concentration of 2900 ppt of ClNO₂ was observed with a mean
30 campaign night-time concentration of 487 ppt, appearing to have an anthropogenic source supported by correlation
31 with SO₂, CO and benzene, which often persisted at high levels after sunrise until midday. This was attributed to
32 such high concentrations persisting after numerous e-folding times of the photolytic lifetime enabling the chlorine
33 atom production to reach 2.3 × 10⁵ molecules cm⁻³ from ClNO₂ alone, peaking at 9:30 am and up to 8.4 × 10⁵
34 molecules cm⁻³ when including the supporting inorganic halogen measurements.

35 Cl-VOCs were measured in the particle and gas phase for the first time at high time resolution and illustrate how
36 the iodide ToF-CIMS can detect unique markers of chlorine atom chemistry in ambient air from both biogenic and
37 anthropogenic sources. Their presence and abundance can be explained via time series of their measured and
38 steady state calculated precursors, enabling the assessment of competing OH and chlorine atom oxidation via
39 measurements of products from both of these mechanisms and their relative contribution to SOA formation.

40

41

42



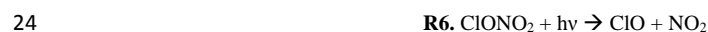
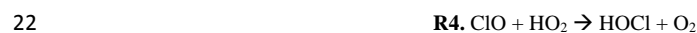
1 1. Introduction

2 NO and NO₂ (NO_x) are important catalysts in the photochemical production of ozone (O₃) playing a significant
3 role in the oxidation of volatile organic compounds (VOCs) and subsequently have an adverse effect on air quality.
4 In the daytime NO_x is primarily removed by the hydroxyl radical (OH) to form nitric acid (HNO₃), which is
5 subsequently lost by wet deposition, becoming a major component of acid rain. At night-time, the OH radical is
6 not a significant oxidant as photolysis stops, enabling the reaction between NO₂ and O₃ to form significant
7 concentrations of the nitrate radical (NO₃) (Atkinson, 2000). NO₃ can accumulate at night or further react with
8 NO₂ leading to the formation of N₂O₅ (Brown *et al.*, 2003b, Brown and Stutz, 2012). This equilibrium can lead to
9 the reaction of NO₃ with VOCs at night forming organic nitrates or act as an important intermediate for
10 heterogeneous reaction on aerosols as N₂O₅ produces NO₃⁻ and NO₂⁺ in the aqueous phase (Hallquist *et al.* 1999,
11 Hallquist *et al.*, 2000, Wagner *et al.*, 2013). In the presence of chlorine, which is assumed in models to
12 predominantly come from sea salt (Baker *et al.*, 2016), nitryl chloride (ClNO₂) can be formed and released into
13 the gas phase from the aerosol surface (Osthoff *et al.*, 2008). ClNO₂ formation thereafter acts as a night-time
14 radical reservoir due to its stability at night.

15 At sunrise ClNO₂ is rapidly photolysed, liberating the highly reactive chlorine atom subsequently converting it
16 into Cl, ClO, HOCl and ClONO₂ depending on the available sunlight, O₃, HO_x and NO_x levels via the following
17 reaction pathways (R1-R9).



19



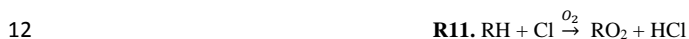
29

30 The liberated chlorine atom can react with VOCs and contribute to daytime photochemical oxidation, competing
31 with OH and perturbing standard organic peroxy radical abundance (RO_x = OH + HO₂ + RO₂), O₃ production rate,
32 NO_x lifetime and partitioning between reactive forms of nitrogen (Riedel *et al.*, 2014). The chlorine atom possesses



1 rate constants with a number of VOCs 200 times larger than OH (Tanaka *et al.*, 2003); therefore, its abundance,
2 fate and cycling can significantly alter standard daytime oxidation pathways. This perturbation is currently thought
3 to only be significant in the early hours of the day while OH concentrations are low and chlorine atom production
4 is high through the photolysis of ClNO₂. Additional Cl₂ photolysis and HCl reaction with OH can also produce
5 chlorine atoms throughout the day but at lower rates.

6 The oxidation mechanism of saturated hydrocarbon (R11-R13) is initiated by reaction with OH or chlorine atom
7 to form an organic peroxy radical (RO₂), and H₂O or HCl depending on the oxidant. In a heavily polluted
8 environment such as Beijing, the RO₂ favours further reactions with NO to form an oxygenated volatile organic
9 compound, HO₂ and NO₂ or an alkyl nitrate RONO₂. Specifically, acyl peroxy radicals can also react with NO₂ to
10 form acyl peroxy nitrates (APN) such as peroxy acetyl nitrate (PAN).



16 Addition of the chlorine atom to unsaturated VOC can also occur and then continue on the similar reaction pathway
17 as R11 – R13. These pathways results in the production of unique chlorine atom chemistry markers which have
18 been previously investigated to indicate the extent of chlorine atom oxidation reactions (Riemer *et al.*, 2008, Keil
19 and Shepson, 2006). The utilization of these compounds, such as 2-chloroperoxypropionyl nitrate (2-Cl PPN) and
20 1-chloro-3-methyl-3butene-2-one (CMBO) as chlorine atom chemistry markers relies on the abundance of the
21 chlorine atom, the VOC precursor; HO_x, NO_x and O₃ and competing pathways for chlorine atom reactions. Riedel
22 *et al.* (2014) calculated that up to tens of ppt Cl-VOCs are formed as a result of chlorine atom addition to alkenes
23 and can therefore provide a number of potential periods of dominating active Cl chemistry (Wang *et al.*, 2001).

24 The production of chloroperoxy radicals via chlorine atom addition can lead to the formation of semi volatile
25 oxidation products which have been observed for both biogenic (Cai and Griffin *et al.*, 2006) and anthropogenic
26 emissions (Huang *et al.*, 2014, Riva *et al.*, 2015) in controlled laboratory studies. Chlorine initiated oxidation of
27 isoprene could also represent a significant oxidation pathway due to its rapid reaction rate compared to OH
28 (Orlando *et al.*, 2003) resulting in gas phase products such as chloroacetaldehyde and CMBO, a unique tracer for
29 atmospheric chlorine atom chemistry (Nordmeyer *et al.*, 1997). Furthermore, reactions of the chlorine atom with
30 isoprene or its SOA derived products could serve as an atmospheric chlorine sink (Ofner *et al.*, 2012). Wang *et al.*
31 (2017) revealed chlorine initiated oxidation of isoprene can produce SOA yields up to 36%, with products similar
32 to that of OH isoprene oxidation. This SOA formation from chlorine initiated oxidation presents a large knowledge
33 gap in the literature, which to date is limited by measurement capabilities.

34 This complex system results in a large uncertainty in the global budget of chlorine atoms ~ 15– 40 Tg Cl yr⁻¹
35 calculated by indirect means (Allan *et al.*, 2007; Platt *et al.*, 2004), which is further limited by the ability of



1 measurement techniques to accurately quantify short lived species at low concentrations. Our knowledge of the Cl
2 budget therefore depends on the accurate measurement of its precursors, namely ClNO₂ and major reaction
3 pathways of the chlorine atom upon liberation in the daytime. Measurements to date show that the concentrations
4 of ClNO₂ vary geographically from below limits of detection to hundreds of ppt (Mielke *et al.*, 2015, Phillips *et*
5 *al.*, 2012, Bannan *et al.*, 2015) and up to 3 ppb (Tham *et al.*, 2014, Riedel *et al.* 2014, Liu *et al.*, 2017) in heavily
6 polluted urban areas. To date, the majority of these measurements have been performed in the United States,
7 although research globally and in China have recently been published (Tham *et al.*, 2014, T Wang *et al.*, 2016, X.
8 Wang *et al.*, 2017, Z. Wang, Liu *et al.* 2017).

9 Iodide adduct ionization has previously been applied to measure inorganic halogens in ambient air (Osthoff *et al.*,
10 2008, Riedel *et al.*, 2012, Thornton *et al.*, 2010, Le Breton *et al.*, 2017) using mass spectrometers with quadrupole
11 mass analysers. This technique involves periodically changing the tuning of the spectrometer to allow transmission
12 of a particular mass ion to the detector. Several species are therefore often “chosen” for detection in order to
13 achieve high enough time resolution. Recent developments and availabilities of a Time of Flight Chemical
14 Ionisation Mass Spectrometer (ToF-CIMS) have enabled the simultaneous measurement of all detectable ions by
15 an ionization technique via high frequency full mass spectral collection. The high resolution (4000) of this
16 technique also enables much lower limits of detection for species which may have the similar mass to a compound
17 that is much more abundant via multi peak fitting. This technique has previously been applied for the measurement
18 of ClNO₂ and Cl₂ (Faxon *et al.* 2015) and recently for Cl-VOCs (Wang *et al.*, 2017) in the gas phase. In this study,
19 a ToF-CIMS utilizing the FIGAERO (Filter Inlet for Gas and AEROSols) is deployed at a site in semi-rural Beijing,
20 China to measure the gas and particle phase precursor (ClNO₂, N₂O₅) and selective halogen containing species at
21 high time frequency and resolution to further our understanding of the chlorine atom budget in this region and its
22 potential fate.

23

24 2. Experimental

25 2.1 Site description

26 The data presented here was collected during the inter-collaborative field campaign, within the framework of a
27 Sino-Sweden research project “Photochemical Smog in China” aimed to further our understanding of the episodic
28 pollution events in China through gas and particle phase measurements with numerous analytical instruments. The
29 laboratory setup in the Changping University Campus of PKU was situated at a semi-rural site 40 km North West
30 of Beijing close to Changping town (40.2207° N, 116.2312° E). The general setup has previously been described
31 by Le Breton *et al.*, 2017.

32

33 All instruments sampled from inlets setup in a laboratory 12 metres high from the 13th May 2016 to 23rd June 2016.
34 The site has a small town within its vicinity and some small factories within 5 kilometers. A High Resolution Time
35 of Flight Aerosol Mass Spectrometer (HR-ToF-AMS) was utilized to measure the mass concentrations and size
36 distributions of non-refractory species in submicron aerosols, including organics, sulfate, ammonium and chloride
37 (DeCarlo *et al.*, 2006, Hu *et al.*, 2013). The setup of this instrument has been previously described by Hu *et al.*,



1 (2016). An Ionicon Analytik high sensitivity PTR-MS (Proton TRansfer Mass Spectrometer) as described by de
2 Gouw and Warneke *et al.*, (2007) provided supporting precursor VOC measurements.

3

4 **2.2 ToF-CIMS setup**

5 Gas and particle phase ambient species were measured using an iodide ToF-CIMS coupled to the FIGAERO inlet
6 (Lopez-Hilfiker *et al.*, 2014). The setup for this campaign has previously been described by le Breton *et al.* (2017).
7 Briefly, the iodide ionization scheme was utilised to acquire non-fragmented ions of interest by passing UHP N₂
8 over a permeation tube containing liquid CH₃I (Alfa Aesar, 99%), and through a Tofwerk X-Ray Ion Source type
9 P (operated at 9.5 kV and 150 μA) to produce the iodide reagent ions. The ionized gas was then carried out of the
10 ion source and into the Ion-Molecule Reaction (IMR) chamber through an orifice (Ø = 1 μm). The inlet lines were
11 2 metres long and composed of copper tubing (12 mm) for the aerosol inlet and Teflon tubing (12 mm) for the gas
12 sample line. Particles were collected onto a Zefluor® PTFE membrane filter at the same rate as the gas inlet line
13 sampling, 2 SLM. The FIGAERO was operated in a cyclic pattern; 25 minutes of gas phase measurement and
14 simultaneous particle collection, followed by a 20 minute period during which the filter was shifted into position
15 over the IMR inlet and the collected particle mass was desorbed.

16

17 **2.4 Calibration**

18 In the field formic acid calibrations were performed daily utilising a permeation source maintained at 40 °C. A dry
19 N₂ flow (200 sccm) was passed over the permeation source and joined a 2 SLM N₂ flow line directed towards the
20 inlet. The concentration of the flow was determined by mass loss in the laboratory after the campaign. The
21 sensitivity of the ToF-CIMS to formic acid was found to be 3.4 ion counts per ppt Hz⁻¹ for 1x10⁵ iodide ion counts.

22 N₂O₅ was synthesized by mixing 20 ppm O₃ with pure NO₂ (98%, AGA Gas) in a glass vessel and then passing
23 the mixture through a cold trap held at -78.5 °C by dry ice. The N₂O₅ was transferred to a diffusion vial fitted with
24 a capillary tube (i.d. 2 mm). The N₂O₅ diffusion source was held at a constant temperature (-23 °C), and the mass
25 loss rate was characterized gravimetrically for a flow rate of 100 sccm. The same flow was added to a dry nitrogen
26 inlet dilution flow of 2 SLM to calibrate the CIMS. ClNO₂ measurements were quantified by passing the N₂O₅
27 over a wetted NaCl bed to produce ClNO₂. The decrease in N₂O₅ from the reaction with NaCl was assumed to be
28 equal to the concentration of ClNO₂ produced (i.e., a 100% yield). Conversion of N₂O₅ to ClNO₂ can be as efficient
29 as 100% on sea salt, but it can also be lower, for example if ClNO₂ were to convert to Cl₂ (Roberts *et al.*, 2008).
30 For NaCl the conversion efficiency has however been as low as 60% (Hoffman *et al.*, 2003). In this calibration we
31 have followed the accepted methods of Osthoff *et al.*, (2008) and Kercher *et al.*, (2009) that show a conversion
32 yield of 100% and have assumed this yield in the calibrations of this study. In this calibration we have followed
33 the accepted methods of Osthoff *et al.*, (2008) and Kercher *et al.*, (2009) that show a conversion yield of 100% and
34 have assumed this yield in the calibrations of this study. The lower detection limit of the CIMS to N₂O₅ and ClNO₂
35 was found to be 9.5 and 1.2 ppt respectively for 1 minute averaged data. Using the error in the individual slope of
36 the calibrations results in a total uncertainty of 30% for both N₂O₅ and ClNO₂. These sensitivities were applied
37 relatively to that of formic acid.



1 A post campaign calibration of chloroacetic acid (99%, Sigma Aldrich) was utilised to apply a sensitivity factor
2 for all Cl-VOCs measured during the campaign. The calibration was performed using the same method as for
3 formic acid and determined a sensitivity of 1.02 ion counts ppt⁻¹ Hz when normalized to 1x10⁵ F ion counts.
4 Relative sensitivities will increase the error to an unknown range, but is a commonly applied method within the
5 CIMS community, although it is likely that the sensitivity is similar for all inorganic/organic halogens, as shown
6 by Le Breton *et al.* (2017).

7

8 **3. Results and Discussion**

9 **3.1 Peak identification and quantification**

10 Peak fitting was performed utilizing the Tofware peak fitting software for molecular weights up to 620 AMU. The
11 standard peak shape was fitted a peak on the spectra until the residual was less than 5%. Each unknown peak was
12 assigned a chemical formula using the peaks exact mass maxima to 5 decimal places and also isotopic ratios of
13 subsequent minor peaks. An accurate fitting was characterized by a ppm error of less than 5 and subsequent
14 accurate fitting of isotopic peaks. The analysis here focuses on species identified in the mass spectra considered to
15 possibly play important roles with respect to the night-time chlorine reservoir and several other key night-time
16 oxidants; ClNO₂, HCl, Cl₂, ClO, HOCl, OClO, ClONO₂, N₂O₅ and Cl-VOCs. Figure 1 displays the average mass
17 spectra for the measurement campaign and the peak fitting applied for ClO and ClNO₂. All species were a dominant
18 peak with a multi peak fit, although a number of co-existing peaks were present for much of the campaign. This
19 signifies the importance of high resolution fit data and the need for high resolution measurements. A quadrupole
20 CIMS may not be able to resolve the peak adjacent to ClO at mass 178 and the second dominant peak for the
21 ClNO₂ fit would result in a 10% over estimation.

22

23 **3.2 N₂O₅ measurements**

24 The CIMS and a Cavity Enhanced Absorption Spectrometer (CEAS) measured N₂O₅ (Wang *et al.*, 2017)
25 simultaneously from the 13th May 2016 to the 6th June 2016. However, given the use of the FIGAERO, the CIMS
26 alternated measurements between gas and particle phases so did not generate a completely continuous gas phase
27 time series. Here, the CEAS is utilised to validate the CIMS N₂O₅ (at m/z 235) measurements and also instrument
28 stability. The CEAS was calibrated for N₂O₅ in the field whereas the CIMS only performed pre and post campaign
29 calibrations. The simultaneous measurements of N₂O₅ can be shown in Figure 2 for one minute averaged data. The
30 time series show a good agreement for both background concentrations during the day (sub 10 ppt) and high night-
31 time concentrations (up to 800 ppt), excluding one night. The highest N₂O₅ levels observed by both the CEAS and
32 CIMS were observed on the 3rd June although the CEAS reports 880 ppt whereas the CIMS reports 580 ppt. If
33 included in the analysis the R² is 0.71 and when excluded it is 0.76. To date the reason for this deviation during
34 that night is not known but it should be stressed that N₂O₅ measurements are delicate and highly depending on
35 sampling condition, e.g. the RH. Nevertheless, excluding this night from the comparison, a slope of 0.85 is
36 observed and a y offset of 0.9. The diurnal profile in Figure 2 represented the difference between the two



1 measurements throughout the campaign. The largest error between the two measurements occurs at night during
2 the higher levels of N_2O_5 , although averaging at 4 ppt. Differences could arise from a number of various factors.
3 Inlet differences such as the CIMS heated IMR (to 40 °C to reduce wall loss), residence time and ambient NO_2 can
4 all change thermal decomposition and wall loss rates between the instruments, which is determined for the CEAS
5 in Wang *et al.* (2017) but not for the CIMS in this work. Also, the inlets were facing in different directions within
6 the same laboratory, possibly enabling local wind patterns to affect the concentrations reaching each instrument.

7 The CEAS data was further utilised to assess any sensitivity changes for the CIMS that daily carboxylic acid
8 calibrations did not account for. A time series of hourly factor differences between the CIMS and CEAS was
9 implemented into the data to weight the measurements to a normalised sensitivity. The high level of agreement
10 from low concentration measurements and a species with a short lifetime from different inlets confirms the
11 accuracy and reliability of the CIMS measurements for this campaign.

12 Generally, N_2O_5 was detected throughout the campaign with a clear diurnal variation peaking at night-time and
13 rapidly falling to below limits of detection in the daytime as a result of photolysis of N_2O_5 and NO_3 . The campaign
14 mean night-time mixing ratio was 121 ppt with a standard deviation of 76 ppt. The maximum concentration of
15 N_2O_5 observed was 880 ppt on the 3rd June. This range of concentrations lie within the recently reported values in
16 the literature, but not at the extreme concentrations as observed in Germany (2.5 ppb) (Phillips *et al.*, 2016) or
17 Hong Kong (7.7 ppb) by Wang *et al.* (2016) and Brown *et al.* (2017). Although the mean concentrations do not
18 increase significantly during the pollution episodes, the maximum concentrations detected overnight increase by
19 up to a factor of 4.

20

21 3.3 Inorganic chlorine abundance and profiles

22 Mean diurnal profiles of HCl, Cl_2 , ClONO_2 , HOCl, ClO and ClNO_2 are displayed in Figure 3 from data between
23 the 23rd May and the 6th June. HCl exhibited a standard diurnal profile increasing in concentration throughout the
24 day and peaking at 4 pm which then fell off slowly at night. The mean HCl campaign concentration was 510 ppt
25 (σ 270 ppt) and the maximum HCl concentration was 1360 ppt on the 30th June. Cl_2 exhibited a diurnal profile
26 peaking at both the night-time and daytime. High concentrations were observed at night followed by a sharp loss
27 at sunrise and a general build-up throughout the day. The campaign mean concentration was 0.65 ppt (σ 0.5 ppt)
28 and the maximum concentration was 4.2 ppt on the 4th June just before midnight. This agrees well with recent
29 urban measurements of Cl_2 in the USA where Faxon *et al.* (2015) observed a maximum of 3.5 ppt and Finley *et al.*
30 (2006) observed up to 20 ppt in California. Up to 500 ppt Cl_2 has recently been reported in the Wangdu County,
31 South West of Beijing (Liu *et al.*, 2017). Although the concentrations we report here are significantly lower, as
32 detailed later, their source maybe of similar origin, which is indicated to be from power plant emissions.

33 The diurnal profile of HOCl peaked during the daytime via its main formation pathways are via reaction of ClO
34 and HO_2 and Cl with OH. Interestingly the ClO in this work exhibits a night-time diurnal peak, contradicting
35 known formation pathways via Cl reaction with O_3 and the photolysis of ClONO_2 . The complexity continues as
36 ClONO_2 also peaks during the night, given that its main known formation pathway is via reaction of ClO (produced
37 at sunrise via ClNO_2 photolysis) with NO_2 . The misidentification of ClONO_2 and ClO is not thought to be a



1 possible reason for these discrepancies due to the low number of mass spectral peaks that have maxima at night
2 and the mass defect of chlorine making the peak position unique to chlorine containing molecules. IMR chemistry
3 is also not a possible source as these reactions would occur throughout the day, therefore skewing all of the data
4 and not just the night-time levels. It is hypothesized that in extremely high OH and HO₂ concentrations, all ClO is
5 rapidly converted to HOCl, limiting the formation on significant levels of ClO and subsequently ClONO₂. Khan
6 *et al* (2008) suggest that Cl atoms of around 2x10⁴ molecules cm⁻³ could be present at night via analysis of alkane
7 relative abundance. Although a formation mechanism is not proposed, it provides further evidence that ClO
8 formation at night-time is possible and may represent an unknown reaction pathway, which would agree with the
9 measurements presented in this work.

10 ClONO₂ exhibited a similar diurnal profile as N₂O₅, peaking at night-time and lost during daylight due to photolysis.
11 The campaign mean night-time mixing ratio was 487 ppt. The maximum concentration observed was 2900 ppt on
12 the 31st May, similar to that previously measured at semi-rural site in Wangdu (up to 1500 ppt) (Liu *et al.*, 2017),
13 Mount Tai (2000 ppt) (Wang *et al.*, 2017), but lower than that in Hong Kong (4 ppb) (Wang *et al* 2016).

14 The high levels of ClONO₂ indicate a local significant source of chlorine to support such high yields. The dominant
15 source of chlorine atoms for ClONO₂ production within models, such as the Master Chemical Mechanism (MCM),
16 is from sea salt, although the site is situated 200 km from the Yellow Sea and therefore has low probability that
17 the Cl has this origin. The mean AMS chloride mass loading was 0.05 μg m⁻³ for the campaign with a maximum
18 of 1.7 μg m⁻³. The Cl⁻ from the AMS appears to be correlated strongly with CO and SO₂, likely to originate from
19 power plants or combustion sources. This suggests the chlorine has an anthropogenic source and not marine, which
20 is also further supported by the wind direction during higher Cl⁻ concentrations (Figure 4). Tham *et al.*, (2016)
21 observed a strong correlation of aerosol chloride with SO₂ and potassium in the same season in 2014 at Wangdu
22 (semi-rural site 160 km south West of Beijing) and suggested contribution to fine chloride from burning of coal
23 and crop residues. The latter was also supported by satellite fire spot count data (Tham *et al.*, 2016). Riedel *et al.*
24 (2013) have previously reported high ClONO₂ concentrations observed from urban and power plant plumes
25 measuring high concentrations of gas phase Cl₂. The correlation with SO₂ indicates coal burning as a potential
26 source of particulate chlorine which is known to be a significant source of PM in the Beijing region (Ma *et al.*,
27 2017), and correlation with CO and benzene is an indicator of biomass burning (Wang *et al.*, 2002).

28 In order to test the hypothesis of biomass burning as a source of particulate chlorine, biomass burning emissions
29 and transport were modelled using the EMEP MSC-W chemical transport model (Simpson *et al.*, 2012, Simpson
30 *et al.*, 2017) driven by meteorology from the WRF-ARW model (Skamarock *et al.*, 2008). The model was run on
31 two nested domains (0.5° and 0.1667° resolution respectively) with biomass burning emissions from the two
32 databases FINN and GFAS, and anthropogenic emissions from the MEIC inventory (<http://meicmodel.org/>). Two
33 versions of the model, one getting emissions from open biomass burning from the Fire Inventory from NCAR
34 (FINN) (Wiedinmyer *et al.*, 2011) and one getting them from the Global Fire Assimilation System (GFAS) (Kaiser
35 *et al.*, 2012), were run for the entire period of the Changping measurement campaign. Neither of these two biomass
36 burning databases contain data on chlorine emissions, so instead the biomass burning emissions of CO (CO_{bb})
37 were tracked and compared to the total concentration of CO (CO_t) at the Changping site. CO was chosen since the
38 measurements at Changping had shown strong correlation between CO and ClONO₂ and because CO could be
39 expected to be co-emitted with chlorine for both biomass burning and industrial combustion.



1 Figure S1 (supplementary) shows time series of the measured ClNO_2 concentrations at the Changping site, as well
2 as the modelled concentrations of CO_t and CO_{bb} . CO_{bb} is shown for both the FINN and GFAS model runs, while
3 CO_t is only shown for the FINN run since it looks almost completely the same for the GFAS run. From this figure
4 it is clear that concentrations of CO_{bb} are very low compared to CO_t . The two episodes of increased concentration,
5 May 18-May 23 and May 28-June 5, are to some extent visible in all time series, but for the biomass burning CO
6 series, the second episode is much less pronounced. Night-time averages of the concentrations shown in figure S2
7 were calculated for each night for the time period 18:00 to 08:00 local time (UTC+8), roughly corresponding to
8 the period when ClNO_2 is not destroyed by photolysis. Nights with significant amount of missing data for the
9 measurements were excluded. Figure S2 shows scatter plots of these averages of ClNO_2 against the averages of
10 the other species. Figure S2 also shows a straight line fitted for each of these scatter plots. The R^2 for these lines
11 were 0.48, 0.04, and 0.21 for CO_t , CO_{bb} FINN, and CO_{bb} GFAS respectively. The fact that concentrations of CO_{bb}
12 is so much smaller than CO_t according to the model, combined with the much better correlation for CO_t than for
13 CO_{bb} strongly suggests that industrial emissions are the dominant source of chlorine, rather than biomass burning.

14 A particle desorption profile was observed in the high resolution data for ClNO_2 . The count increase at this 1 AMU
15 mass can be attributed to two sources; SO_3 and ClNO_2 as shown in Figure 5. The SO_3 peak is predominantly found
16 in the particle phase and is below limit of detection (LOD) in the gas phase. During initial analysis of the data,
17 SO_3 interfered with the ClNO_2 peak fitting and attributed its counts to ClNO_2 in the particle phase as its ^{33}S ion is
18 only 0.005 AMU away from the ClNO_2 peak. Upon its inclusion into the peak list and utilisation of the Tofware
19 feature which constrains isotopes and reallocates the signal appropriately, ClNO_2 remains to indicate a strong
20 desorption profile. The diurnal cycle of these desorptions correlate well with the ClNO_2 gas phase profile,
21 indicating a correct assignment of the counts to particle phase ClNO_2 . The desorption profiles with respect to
22 temperature also exhibit a thermogram structure and not e.g. a gas phase leak into the system which could have
23 accounted for the correlation with the gas phase time series. This suggests the possible presence of ClNO_2 in the
24 particle phase. Another possible explanation could be the deposition of ClNO_2 from the gas phase onto the filter
25 as the ambient air flows through the FIGAERO.

26 If we assume the analysis and collection technique is correct, we see an average particle to gas phase partitioning
27 of 0.07, with a maximum of 0.33 and a minimum of 0.009. The average concentration of ClNO_2 collected onto the
28 filter during desorption is 13 ppt with a maximum of 120 ppt. Previous modelling studies assume all ClNO_2 is in
29 the gas phase due to the low Henry's law constant e.g. for the TexAQ5 II campaign they calculated that 0.1 ppb
30 in the gas phase would yield 0.54 ppt in the particle phase (Simon *et al.*, 2008). However, these data indicates a
31 significant amount of the chlorine associated with ClNO_2 is not liberated from the particle phase. The slope of the
32 particle to gas phase CIMS data is calculated to be 0.048, a factor of 96 higher than using the Henry's law
33 coefficient to estimate the particle concentration.

34

35 3.4 ClNO_2 daytime persistence and Cl liberation

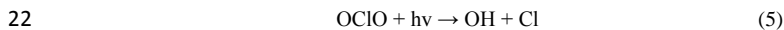
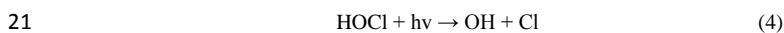
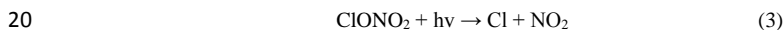
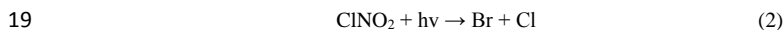
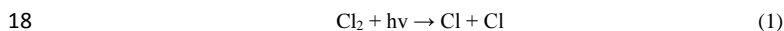
36 Both ClNO_2 and N_2O_5 are photochemically unstable, with studies reporting lifetimes on the order of hours for ClNO_2
37 depending on the solar strength (e.g. Ganske *et al.*, 1992, Ghosh *et al.*, 2011). Nocturnal ClNO_2 removal pathways
38 have generally been reported to be negligible, with ClNO_2 being assumed to be relatively inert (Wilkins *et al.*,



1 1974; Frenzel et al., 1998; Rossi, 2003; Osthoff et al., 2008), but the work of Roberts et al., (2008) and Kim et al.,
 2 (2014) would suggest that this may not be strictly true. However, given that the average diurnal profile does not
 3 show the importance of nocturnal removal pathways in this study, observed losses are attributed solely to
 4 photolysis, with $J(\text{ClNO}_2)$ controlling the lifetime.

5 Rapid photolysis can be observed for N_2O_5 in Figure 6 showing a near instant drop below LOD, whereas the ClNO_2
 6 concentration not only persists for up to 7 hours, but also shows evidence of an increase in concentration at 7 am
 7 (Figure 6). This is observed throughout the campaign and has been frequently observed in the previous study at
 8 Wangdu (Tham *et al.*, 2016). The breakdown of the nocturnal boundary layer and inflow of air masses from above,
 9 carrying pollution from nearby industry/ies is a likely cause of this persistence of possible increase of ClNO_2 . Liu
 10 *et al.* (2017) also observed high daytime concentrations of ClNO_2 (60 ppt) at the Wangdu site which they attribute
 11 to a possible oxidation mechanism due its correlation with O_3 and Cl_2 providing a daytime formation pathway to
 12 maintain concentrations against its rapid photolysis.

13 Consistent with past measurements and the measurements of this study, ClNO_2 is expected to provide a significant
 14 source of Cl during day time hours, presenting a potentially significant source of the reactive Cl atom during the
 15 day. Its rapid photolysis rate and elevated concentrations enables Cl to compete with OH oxidation chemistry, the
 16 known dominant daytime radical source. Here, a simple steady state calculation will be used to determine the Cl
 17 atom concentration as detailed;



$$25 \quad [\text{Cl}]_{\text{steady state}} = \{2J_1[\text{Cl}_2] + J_2[\text{ClNO}_2] + J_3[\text{ClONO}_2] + J_4[\text{HOCl}] + J_5[\text{OCIO}]\} / \{k_6[\text{O}_3] + k_7[\text{CH}_4_{\text{equivalent}}]\}$$

26 Where $[\text{CH}_4]_{\text{equivalent}}$ represents the reactive VOC present as if it were equivalent CH_4

27 Steady state calculations reveal a sharp rise of chlorine atoms produced at sunrise peaking at 1.6×10^5 molecules
 28 cm^3 around 7 am which then gradually decreases, contributing to Cl atom production until 2 pm (Figure 7a).
 29 Supporting Cl_2 , ClONO_2 , OCIO , HOCl and HCl measurements by CIMS report that chlorine atoms can sustain a
 30 relatively high production rate until 3 pm as evidenced by the daytime build-up of HCl and Cl_2 . ClNO_2 on average
 31 contributes to 78% of the chlorine atoms produced from inorganic halogens with 13% from Cl_2 . ClNO_2 also
 32 represents over 50% of the chlorine atoms until midday. After ca. 3 pm Cl_2 and HCl becomes the more dominant
 33 Cl atom source. On the night where the highest ClNO_2 concentrations were measured, 90% of the chlorine atoms
 34 originated from ClNO_2 photolysis until 2 pm and HCl and Cl_2 then become main contributors sustaining until 4



1 pm (up to 80%). ClONO₂, HOCl and OClO appear to be insignificant contributors to chlorine atom throughout the
2 campaign compared with ClNO₂, HCl and Cl₂.

3 To put these chlorine atom concentrations into a more global perspective, data collected by the University of
4 Manchester from a marine site and an urban European site have been compared in Figure 7b. Bannan *et al.*, (2015)
5 and (2017) previously utilised a box model to calculate Cl atom concentrations during the campaign so that the
6 rate of oxidation of VOCs by Cl atoms could be compared with oxidation by measured OH and measured ozone.
7 The simple steady state calculation described previously will be used to determine the Cl atom concentration for
8 both this measurement study.

9 The results show that both at the UK marine and urban site max chlorine atom concentrations are more than an
10 order of magnitude lower than the mean of Beijing. It should however be noted that the only source of Cl in the
11 UK studies was ClNO₂, but given the dominance of ClNO₂ in this study the measurements presented here suggest
12 a high importance of the chlorine chemistry for the Asian air chemistry.

13 Although this study does not reach the scope of characterising O₃ and RO_x production from chlorine atom
14 chemistry, statistics are often reported with ClNO₂ morning chemistry via modelling simulations, we can put into
15 perspective the mean and maximum concentrations relative to other studies. Tham *et al.* (2016) recorded a
16 maximum ClNO₂ concentration of 2070 ppt from a plume originating from Tianjin, the closest megacity to Beijing,
17 and report a 30% increase in RO_x production and up to 13% of O₃ production. Liu *et al.* (2017) observed peak
18 concentrations up to 3 ppb and similar diurnal concentrations which they calculated contributes to a 15%
19 enhancement of peroxy radicals and 19% O₃ production. Wang *et al.* (2016) report up to 4.7 ppb of ClNO₂ in Hong
20 Kong and calculated a maximum increase of 106% of HO_x in the morning and an enhancement of following
21 daytime O₃ production up to 41%. It is therefore evident that this work supports similar studies in Asia that
22 conclude that chlorine atom oxidation significantly contributes to atmospheric oxidation via RO_x and O₃
23 production. This consistent result in Asia cannot be drawn globally as a number of studies have deemed chlorine
24 atom chemistry to be insignificant with respect to O₃ production and competing VOC oxidation to OH (Bannan
25 *et al.*, 2017), implying a significantly different approach is needed to assessing oxidation chemistry and
26 photochemical smog in Asia (Hallquist *et al.* 2016).

27

28 3.5 VOC oxidation by chlorine atoms

29 Steady state calculations of OH (as described by Whalley *et al.*, 2010) estimate that campaign average maximum
30 concentration was 7×10^6 molecules cm³ (Figure 7b), 6 times greater than the maximum chlorine atom
31 concentration and 14 times higher than the average chlorine atom concentration. Pszenny *et al.* (2007) report
32 estimated OH to chlorine atom ratios, from VOC lifetime variability relationships, of 45 to 199 along the East
33 Coast of the United States. Although the ratio appears much larger than calculated in this work, here we present
34 not only significantly high concentrations of ClNO₂ which are appearing to be a consistent conclusion from
35 measurements in Asia, but also the chlorine within this study appears to originate from an anthropogenic origin
36 rather than marine, possessing the ability to supply a much larger reservoir of halogens to be liberated through
37 photolysis.



1 The relative oxidation rate of the chlorine atom and OH to VOCs can vary greatly. Rate coefficients for reaction
2 of Cl atoms with some volatile organic compounds have been shown to be up to 200 times faster than the
3 comparable reaction with OH. The ratio reported here is significantly less than this each day, Cl can subsequently
4 dominate VOC oxidation for some fraction of the day. Here, the diurnal maxima of the chlorine atom and OH
5 differs by 5 hours, enabling chlorine atoms to clearly dominate VOC oxidation earlier in the day before OH
6 concentrations have built up. The relative oxidation rate of VOCs to OH and the chlorine atom also varies greatly,
7 creating a difference for various VOCs. If an average reaction rate for alkenes and alkanes to Cl and OH is
8 calculated, it is possible to generalise the significance of each oxidation pathway to qualitatively assess the
9 contribution chlorine atoms have on oxidation chemistry. It can be seen in Figure 8 that alkenes are much more
10 likely to be oxidised by OH than Cl, although a significant contribution (15%) is attributed to chlorine chemistry.
11 Although significant if evaluated on a global level, Liu *et al.*, (2017) estimated that Cl atoms oxidize slightly more
12 alkanes than OH radicals in a similar region of China, implying the increased scale of chlorine oxidation in China.
13 Alkanes are known to have a much higher Cl to OH relative reaction rate than alkenes and Cl contribution to
14 oxidation is higher than OH until midday. The contribution to oxidation remains almost equal for the remainder
15 of the day due to the persistence of ClNO₂ and also relatively high levels of Cl₂ and HCl. This analysis is
16 representative of that by Bannan *et al.* (2015) who report contributions of alkene and alkane oxidation by Cl up to
17 3 and 15% respectively from ClNO₂ concentrations peaking at 724 ppt.

18 This significant oxidation of VOCs by chlorine atoms will result in different products to that of OH oxidation as
19 illustrated that neglecting the contributions made by Cl atoms will significantly underestimate the degree of
20 chemical processing of VOCs in this study, and other environments where there is a source of Cl atoms. Evidence
21 of the proposed Cl oxidation of VOCs is validated through detection of selected Cl induced oxidation products by
22 the ToF-CIMS, all of which are displayed in Table 1.

23

24 3.5.1 Isoprene oxidation by the chlorine atom

25 1-Chloro-3-methyl-3-butene-2-one (CMBO, C₅H₆ClO), a unique marker of chlorine-isoprene reactions, has
26 previously been measured at concentrations up to 9 ppt by offline gas chromatography in Houston Texas (Tanaka
27 *et al.*, 2003) and in laboratory studies of chlorine-isoprene oxidation (Wang *et al.* (2017)). CMBO exhibited a
28 campaign maximum of 13.2 ppt and mean of 5.16 ppt exhibiting a near typical diurnal profile with concentrations
29 rising sharply after sunrise, at the same rate as the chlorine atom production but maintaining concentrations past
30 noon longer than that of isoprene and the chlorine atom, due to its longer atmospheric lifetime.

31 The daily maxima of CMBO varied throughout the campaign and can be explained by the relative concentrations
32 of its precursors; the chlorine atom and isoprene. Its concentration throughout the campaign followed similar
33 intensities to its precursors and figure 9 highlights its dependence on both Cl atom and isoprene concentrations.
34 The concentrations of Cl and isoprene were relatively low from the 24th to the 27th of May, which resulted in
35 relatively low CMBO concentrations. An increase in isoprene and Cl on the 28th to the 30th May was subsequently
36 mirrored by the CMBO levels as qualitatively expected. On closer inspection of the 30th and 31st May, the
37 concentration of CMBO was lower than expected on the 30th due to higher chlorine atom and isoprene
38 concentrations compared to the 31st. This could be explained by anticipated higher OH concentration as calculated



1 by the steady state model, which is also further represented by higher concentrations of IEPOX (isoprene
2 epoxydiols, i.e. OH oxidation products) on the 30th. This illustrates how the ToF-CIMS can identify isoprene
3 oxidation products of two competing oxidation pathways. The high levels of IEPOX on the 28th May can also
4 possibly describe the relatively high levels of CMBO in the particle phase due to an already well oxidised air mass.

5 Further daily oxidation rates can be probed via analysis of the related isoprene oxidation products observed by the
6 CIMS. Figure 10 depicts the diurnal time series of the precursor itself and several Cl-VOC products and IEPOX.
7 CMBO concentrations rise rapidly after sunrise due to the low concentration of OH and high production rate of
8 the chlorine atom. The secondary and tertiary products, C₅H₉ClO₂ and C₅H₉ClO₃ (also measured in the laboratory
9 by Wang *et al.*, 2017) increased in concentration at a much slower rate, but appear to peak later in the day (4 pm)
10 whereas CMBO peaked around 10 am (similar to the ClNO₂ peak time) and fall off, due to its further oxidation to
11 form the secondary and tertiary products. IEPOX concentrations increased slowly after sunrise and peaked later in
12 the day, as expected due to the availability of OH and competition from the chlorine atom chemistry. The similar
13 time series of the secondary and tertiary products to IEPOX was also reported by Wang *et al.*, (2017) and were
14 suggested to be ideal tracers of SOA production.

15

16 3.5.2 Anthropogenic Cl-VOC production

17 A similar unique chlorine oxidation marker in urban coastal areas, has been reported in the literature for 1, 3
18 butadiene; 4-chlorocrotonaldehyde (CCA) (Wang *et al.*, 2000). No measurements of 1, 3 butadiene were made
19 during this field campaign, although due to its common source to benzene (automobile exhausts (Ye *et al.*, 1998),
20 we present a comparison of the CCA measured by CIMS and benzene measurements made by the PTR-MS. The
21 intensity of CCA in both the gas and particle phase with concentration in the gas phase up to 13 ppt reflect well
22 the concentrations of its precursors. The maximum concentration of the chlorine atom coincides with a high
23 concentration of benzene and subsequently CCA on the 30th May whereas very low levels of CCA were observed
24 for the beginning of the campaign (Figure 11).

25 The diurnal time series of benzene (Figure 12) indicates high concentrations in the early hours of the day, possibly
26 associated with high anthropogenic activity or an inflow of urban air masses from downtown Beijing. The
27 concentration falls off throughout the day and almost perfectly anti correlates with the CCA gas phase diurnal
28 profile which increases from sunrise and peaks at 3 pm. The particle phase CCA diurnal time series steadily builds
29 up throughout the day and do not peak until late in the evening, providing evidence of SOA production from the
30 chlorine oxidation of anthropogenic pollutants.

31

32 4. Conclusions

33 A FIGAERO ToF-CIMS was utilised in Beijing to assess the liberation of chlorine atoms via inorganic halogen
34 photolysis. A suite of inorganic halogens were detected, namely ClNO₂ reaching concentrations up to 2900 ppt,
35 which is suggested to have an anthropogenic origin due to the particulate chlorine correlation with SO₂, benzene
36 and CO. ClNO₂ was potentially identified in the particle phase, which may only prove to be significant at such



1 elevated concentrations as observed in East Asia. ClNO₂ concentrations above LOD persisted up to 7 hours past
2 sunrise, attributed to the lifetime of ClNO₂ at these high concentrations and a possible in-flow of heavily polluted
3 air masses from the downtown urban area. Supporting Cl₂ and HCl concentrations proved to be significant
4 contributors to chlorine atom production via steady state calculations enabling an average daytime peak
5 concentration of chlorine atoms of 1.6 x10⁵ molecules cm⁻³. Compared with data attained from European based
6 campaigns, these concentrations exceed marine and urban environments by at least an order of magnitude.

7 This high concentration of chlorine atoms resulted in a steady state calculated OH:Cl ratios down to a factor of 6,
8 enabling Cl chemistry to not only dominate alkane oxidation until midday but contribute significantly to alkene
9 oxidation throughout the day (15% on average). This enabled significant concentrations of Cl-VOCs to be formed
10 providing the first ambient high time resolution measurements of specific Cl-VOC species simultaneously
11 measured in the gas and particle phase. The measured unique markers of chlorine chemistry for both biogenic and
12 anthropogenic precursors provides quantitative and qualitative data to probe the extent of chlorine atom chemistry
13 and how they compete with OH. Simultaneous measurements of the VOC precursors via PTR-MS, and IEPOX,
14 Cl-VOCs with the CIMS provides rich information on SOA formation pathways via both OH and chlorine atom
15 oxidation. Multistep oxidation products of Cl-VOCs were also identified and can provide partitioning information
16 and SOA formation rates and lifetimes.

17 The results highlight how chlorine atom chemistry may be under represented within models due to the lack of
18 quantification and identification of particulate Cl-VOC products. This work provides instrumental capability to
19 probe the competition between OH and Cl oxidation chemistry and quantify the SOA yields as a result of both
20 pathways.

21

22 **Acknowledgement:**

23 The work was done under the framework research program on ‘Photochemical smog in China’ financed by
24 Swedish Research Council (639-2013-6917). The National Natural Science Foundation of China (21677002) and
25 the National Key Research and Development Program of China (2016YFC0202003) also helped fund this work.

26

27 **References**

28 Allan, W., Struthers, H. and Lowe, D. C.: Methane carbon isotope effects caused by atomic chlorine in the marine
29 boundary layer: Global model results compared with southern hemisphere measurements. *J. Geophys. Res.* 112,
30 2007.

31 Baker, A. K., Sauvage, C., Thorenz, U. R., van Velthoven, P., Oram, D. E., Zahn, A., Berninkmeijer, C. A. M.
32 and Williams, J.: Evidence for strong, widespread chlorine atom chemistry associated with pollution outflow
33 from continental Asia, *Sci. Rep.*, 6, 36821, 2016.

34 Bannan, T. J., Booth, A. M., Bacak, A., Muller, J. B. A., Leather, K. E., Le Breton, M., Jones, B., Young, D., Coe,
35 H., Allan, J., Visser, S., Slowik, J. G., Furger, M., Prevot, A. S. H., Lee, J., Dunmore, R. E., Hopkins, J. R.,
36 Hamilton, J. F., Lewis, A. C., Whalley, L. K., Sharp, T., Stone, D., Heard, D. E., Fleming, Z. L., Leigh, R.,
37 Shallcross, D. E., and Percival, C. J.: The first UK measurements of nitryl chlorine using a chemical ionization



- 1 mass spectrometer in central London in the summer of 2012, and an investigation of the role of Cl atom oxidation,
2 J. Geophys. Res. Atmos., 120, 5638–5657, 2015.
- 3 Bannan, T. J., Bacak, A., Le Breton, M., Ouyang, B., Flynn, M., McLeod, M., Jones, R., Malkin, T. L., Whalley,
4 L. K., Heard, D. E., Bandy, B., Khan, A., Shallcross, D. E., and Percival, C. J.: Ground and airborne U.K.
5 measurements of nitryl chloride, an investigation of the role of Cl atom oxidation at Weybourne Atmospheric
6 Observatory, J. Geophys. Res. Atmospheres, 10.2017.
- 7 Brown, S. S. & Stutz, J. Nighttime radical observations and chemistry Chem. Soc. Rev., The Royal Society of
8 Chemistry, 41, 6405-6447, 2012.
- 9 Cai, X., Ziemba, L. D. and Griffin, R. J.: Secondary aerosol formation from the oxidation of toluene by chlorine
10 atoms, Atmos. Environ., 42, 32, 2008.
- 11 Brown, S. S., Stark, H., and Ravishankara, A. R.: Applicability of the steady state approximation to the
12 interpretation of atmospheric observations of NO₃ and N₂O₅, J. Geophys. Res. - Atmos., 108, 4539, 2003.
- 13 Brown, S. S., Dube, W. P., Tham, Y. J., Zha, Q. Z., Xue, L. K., Poon, S., Wang, Z., Blake, D. R., Tsui, W., Parrish,
14 D. D., Wang, T.: Nighttime chemistry at a high altitude site above Hong Kong, J. Geophys. Res. Atmos., Vol. 121,
15 Issue. 5, 2457-2475, 2016.
- 16
- 17 DeCarlo, P. F., Kimmel, J., Trimborn, A., Northway, M., Jayne, J. T., Aiken, A., Gonin, M., Fuhrer, K., Horvath,
18 T., Docherty, K., Worsnop, D. R., and Jimenez, J. L.: Field-deployable, high-resolution, time-of-flight Aerosol
19 Mass Spectrometer, Anal. Chem., 78, 8281–8289, 2006.
- 20 de Gouw, J. and Warneke, C.: Measurements of volatile organic compounds in the earth's atmosphere using
21 proton-transfer-reaction mass spectrometry, Mass Spectrom. Rev., 26, 223–257, 2007.
- 22 Faxon, C. B., Bean, J. K., and Ruiz, L. H.: Inland Concentrations of Cl₂ and ClNO₂ in Southeast Texas suggest
23 chlorine chemistry significantly contributes to atmospheric reactivity, Atmosphere, 6, 1487–1506, 2015.
- 24 Finley, B. D. and Saltzman, E. S: Measurement of Cl₂ in coastal urban air, Geophys. Res. Lett., 33, 2006.
- 25 Hoffman, R. C., Gebel, M. E., Fox, B. S., and Finlayson-Pitts, B. J.: Knudsen cell studies of the reactions of
26 N₂O₅ and ClONO₂ with NaCl: Development and application of a model for estimating available surface areas
27 and corrected uptake coefficients, Phys. Chem. Chem. Phys., 5, 9, 1780–1789, 2003.
- 28 Hu, W. W., Hu, M., Yuan, B., Jimenez, J. L., Tang, Q., Peng, J. F., Hu, W., Shao, M., Wang, M., Zeng, L. 74 M.,
29 Wu, Y. S., Gong, Z. H., Huang, X. F., and He, L. Y.: Insights on organic aerosol aging and the influence of
30 coal combustion at a regional receptor site of central eastern China, Atmos. Chem. Phys., 13, 10095-10112,
31 2013.
- 32 Hu, W., Hu, M., Hu, W., Jimenez, J. L., Yuan, B., Chen, W., Wang, M., We, Y., Chen, C., Wang, Z., Peng, J.,
33 Zeng, L. and Shao, M. Chemical composition, sources, and aging process of submicron aerosols in Beijing:
34 Contrast between summer and winter, J. Geophys. Res., 121, 4, 1955-1977, 2016.
- 35 Huang, M., Liu, X., Hu, C., Guo, X., Gu, X., Zhao, W., Wang, Z., Fang, L. and Zhang, W.: Aerosol laser time-of-
36 flight mass spectrometer for the on-line measurement of secondary organic aerosol in smog chamber, Meas. J. Int.
37 Meas. Confed., 55(3), 394–401, 2014.
- 38 Keil, A. and Shepson, P.: Chlorine and bromine atom ratios in the springtime Arctic troposphere as determined
39 from measurements of halogenated volatile organic compounds, J. Geophys. Res., 111, 2006.
- 40 Kercher, J. P., Riedel, T. P., and Thornton, J. A.: Chlorine activation by N₂O₅: simultaneous, in situ detection of
41 ClONO₂ and N₂O₅ by chemical ionization mass spectrometry, Atmos. Meas. Tech., 2, 193–204, doi:10.5194/amt-
42 2-193-2009, 2009.



- 1 Khan, M. A. H., Ashfold, M. J., Nickless, G., Martin, D., Watson, L. A., Hamer, P. D., Wayne, R. P., Canosa-
2 Mas, C. E. and Shallcross, D. E.: Night-time NO₃ and OH radical concentrations in the United Kingdom inferred
3 from hydrocarbon measurements, *Atmos. Sci. Lett.*, 9, 3, 140-146, 2008.
- 4 Lopez-Hilfiker, F. D., Mohr, C., Ehn, M., Rubach, F., Kleist, E., Wildt, J., Mentel, Th. F., Lutz, A., Hallquist, M.,
5 Worsnop, D., and Thornton, J. A.: A novel method for online analysis of gas and particle composition: description
6 and evaluation of a Filter Inlet for Gases and AEROSols (FIGAERO), *Atmos. Meas. Tech.* 2014, 7, 983–1001,
7 doi:10.5194/amt-7-983-2014.
- 8 Le Breton, M, Bannan, T. J., Shallcross, D. E., Khan, M. A., Evans, M. J., Lee, J., Lidster, R., Andrews, S.,
9 Carpenter, L., Schmidt, J., Jacob, D., Harris, N. R. P., Bauguitte, S-J., Gallagher, M., Bacak, A., Leather, K. E.
10 and Percival, C. J.: Enhanced ozone loss by active inorganic bromine chemistry in the tropical troposphere, *Atmos.*
11 *Environ.*, 155, 21-28, 2017.
- 12 Le Breton, M., Wang, Y., Hallquist, Å. M., Pathak, R. K., Zheng, J., Yang, Y., Shang, D., Glasius, M., Bannan,
13 T. J., Liu, Q., Chan, C. K., Percival, C. J., Zhu, W., Lou, S., Topping, D., Wang, Y., Yu, J., Lu, K., Guo, S., Hu,
14 M., and Hallquist, M.: Online gas and particle phase measurements of organosulfates, organosulfonates and
15 nitrooxyorganosulfates in Beijing utilizing a FIGAERO ToF-CIMS, *Atmos. Chem. Phys. Discuss.*,
16 <https://doi.org/10.5194/acp-2017-814>, in review, 2017.
- 17 Lopez-Hilfiker, F. D., Mohr, C., Ehn, M., Rubach, F., Kleist, E., Wildt, J., Mentel, Th. F., Lutz, A., Hallquist, M.,
18 Worsnop, D., and Thornton, J. A.: A novel method for online analysis of gas and particle composition: description
19 and evaluation of a Filter Inlet for Gases and AEROSols (FIGAERO), *Atmos. Meas. Tech.* 2014, 7, 983–1001,
20 doi:10.5194/amt-7-983-2014.
- 21 Ma, Q., Shuxiao, S. C., Zhao, B., Martin, R. V., Brauer, M., Cohen, A., Jiang, J., Zhou, W., Hao, J., Frostad, J.,
22 Forouzanfar, M. H. and Burnett, T.: Impacts of coal burning on ambient PM₁ pollution in China, *Atmos. Chem.*
23 *Phys.*, 17, 4477-4491, 2017.
- 24 Mielke, L. H., Furgeson, A., Odame-Ankrah, C. A., and Osthoff, H. D.: Ubiquity of ClNO₂ in the urban boundary
25 layer of Calgary, AB, Canada, *Canadian J. Chem.*, 2015.
- 26 Nordmeyer, T., Wang, W., Ragains, M. L., Finlayson-Pitts, B. J., Spicer, C. W. and Plastringe, R. A.: Unique
27 products of the reaction of isoprene with atomic chlorine: Potential markers of chlorine atom chemistry, *Geophys.*
28 *Res. Lett.*, 24(13), 1615–1618, doi:10.1029/97GL01547, 1997.
- 29 Ofner, J., Balzer, N., Buxmann, J., Grothe, H., Schmitt-Kopplin, P., Platt, U. and Zetzsch, C.: Halogenation
30 processes of secondary organic aerosol and implications on halogen release mechanisms, *Atmos. Chem. Phys.*,
31 12(13), 5787–5806, doi:10.5194/acp-12-5787-2012, 2012.
- 32 Orlando, J. J., Tyndall, G. S., Apel, E. C., Riemer, D., and Paulson, S. E.: Rate coefficients and mechanisms of the
33 reaction of Cl-atoms with a series of unsaturated hydrocarbons under atmospheric conditions, *Int. J. Chem. Kinet.*,
34 35, 334–353, 2003.
- 35 Osthoff, H.D.; Roberts, J.M.; Ravishankara, a. R.; Williams, E.J.; Lerner, B.M.; Sommariva, R.; Bates, T.S.;
36 Coffman, D.; Quinn, P.K.; Dibb, J.E.: High levels of nitryl chlorine in the polluted subtropical marine boundary
37 layer. *Nat. Geosci.* 2008, 1, 324–328, 2008.
- 38 Platt, U., Allan, W., and Lowe, D.: Hemispheric average Cl atom concentration from 13C/12C ratios in
39 atmospheric methane, *Atmos. Chem. Phys.*, 4, 2393–2399, 4, 2004.
- 40 Phillips, G. J., Tang, M. J., Thieser, J., Brickwedde, B., Schuster, G., Bohn, B., Lelieveld, J., and Crowley, J. N.:
41 Significant concentrations of nitryl chlorine observed in rural continental Europe associated with the influence of
42 sea salt chlorine and anthropogenic emissions, *Geophys. Res. Lett.*, 39, L10811, 2016.



- 1 Phillips, G. J., Thieser, J., Tang, M., Sobanski, N., Schuster, G., Fachinger, J., Drewnick, F., Borrmann, S.,
2 Bingemer, H., Lelieveld, J. and Crowley, J. N.: Estimating N_2O_5 uptake coefficients using ambient measurements
3 of NO_3 , N_2O_5 , ClNO_2 and particle-phase nitrate, *Atmos. Chem. Phys.*, 16, 13231-13249, 2016.
- 4 Pszenny, A. A. P., Fischer, E. V., Russo, R. S., Sive, B. C., and Varner, R. K.: Estimates of Cl atom concentrations
5 and hydrocarbon kinetic reactivity in surface air at Appledore Island, Maine (USA), during International
6 Consortium for Atmospheric Research on Transport and Transformation/Chemistry of Halogens at the Isles of
7 Shoals, *J. Geop.*
- 8 Riedel, T. P., Bertram, T. H., Crisp, T. A., Williams, E. J., Lerner, B. M., Vlasenko, A., Li, S. M., Gilman, J., de
9 Gouw, J., Bon, D. M., Wagner, N. L., Brown, S. S., and Thornton, J. A.: Nitryl chlorine and molecular chlorine in
10 the coastal marine boundary layer, *Environ. Sci. Technol.*, 46, 10463–10470, 2012.
- 11 Riedel, T. P., Wolfe, G. M., Danas, K. T., Gilman, J. B., Kuster, W. C., Bon, D. M., Vlasenko, A., Li, S. M.,
12 Williams, E. J., Lerner, B. M., Veres, P. R., Robert, J. M., Holloway, J. S., Lefer, B., Brown, S.S. and Thornton,
13 J. A.: An MCM modeling study of nitryl chlorine (ClNO_2) impacts on oxidation, ozone production and nitrogen
14 oxide partitioning in polluted continental outflow, *Atmos. Chem. Phys.*, 14, 3789-3800, 2014.
- 15 Riemer, D. D., Apel, E. C., Orlando, J. J., Tyndall, G. S., Brune, W. H., Williams, E. J., Lonneman, W. A. and
16 Neece, J. D.: Unique isoprene oxidation products demonstrate chlorine atom chemistry occurs in the Houston,
17 Texas urban area, *J. Atmos. Chem.*, 61(3), 227–242, 2008.
- 18 Riva, M., Healy, R. M., Flaud, P. M., Perraudin, E., Wenger, J. C. and Villenave, E.: Gas- and Particle-Phase
19 Products from the Chlorine-Initiated Oxidation of Polycyclic Aromatic Hydrocarbons, *J. Phys. Chem. A*, 119(45),
20 11170–11181, doi:10.1021/acs.jpca.5b04610, 2015.
- 21 Roberts, J. M., Osthoff, H. D., Brown, S. S., and Ravishankara, A. R.: N_2O_5 oxidizes chloride to Cl_2 in acidic
22 atmospheric aerosol, *Science*, 321, 1059–1059, doi:10.1126/science.1158777, 2008.
- 23 Sander, R.: Modeling atmospheric chemistry: Interactions between gas-phase species and liquid cloud/aerosol
24 particles, *Surv. Geophys.*, 20, 1–31, 1999.
- 25 Simon, H., Y. Kimura, G. McGaughey, D.T. Allen, S.S. Brown, H.D. Osthoff, J.M. Roberts, 422 D. Byun, and D.
26 Lee.: Modeling the impact of ClNO_2 on ozone formation in the 423 Houston area, *J. Geophys. Res.*, 114, D00F03,
27 424 doi:10.1029/2008JD010732, 2009.
- 28 Tanaka, P. L., Riemer, D. D., Chang, S., Yarwood, G., McDonaldBuller, E. C., Apel, E. C., Orlando, J. J., Silva,
29 P. J., Jimenez, J. L., Canagaratna, M. R., Neece, J. D., Mullins, C. B., and Allen, D. T.: Direct evidence for
30 chlorine-enhanced urban ozone formation in Houston, Texas, *Atmos. Environ.*, 37, 1393–1400, 2003.
- 31 Tham, Y., Yan, C., Xue, L., Zha, Q., Wang, X., and Wang, T.: Presence of high nitryl chlorine in Asian coastal
32 environment and its impact on atmospheric photochemistry, *China Sci. Bull.*, 59, 356–359, doi:10.1007/s11434-
33 013-0063-y, 2014.
- 34 Thornton, J. A., Kercher, J. P., Riedel, T. P., Wagner, N. L., Cozic, J., Holloway, J. S., Dube, W. P., Wolfe, G. M.,
35 Quinn, P. K., Middlebrook, A. M., Alexander, B., and Brown, S. S.: A large atomic chlorine source inferred from
36 mid-continental reactive nitrogen chemistry, *Nature*, 464, 271–274, doi:10.1038/nature08905, 2010.
- 37 Wagner, N. L., Riedel, T. P., Young, C. J., Bahreini, R., Brock, C. A., Dube, W. P., Kim, S., Middlebrook, A. M.,
38 Öztürk, F., Robert, J. M., Russo, R., Sive, B., Swarthout, R., Thornton, J. A., VandenBoer, T. C., Zhou, Y. and
39 Brown, S. S.: N_2O_5 uptake coefficients and nocturnal NO_2 removal rates determined from ambient wintertime
40 measurements, *Atmos. Chem. Phys.*, 11, 9331-9350, 2013.
- 41 Wang, W. and Finlayson-Pits, B. J.: Unique markers of chlorine atom chemistry in coastal urban areas: The
42 reaction with 1,3-butadiene in air at room temperature, *J. Geophys. Res.*, 106, 5, 4939-4958, 2001.



- 1 Wang, T., Cheung, T., Li, Y., Yu, X. and Blake, D.: Emission characteristics of CO, NO_x, SO₂ and indications of
2 biomass burning observed at a rural site in eastern China. *J. Geophys. Res. Atmos.*, 107, 12, 2002.
- 3 Wang, T., Tham, Y.J., Xue, L., Li, Q., Zha, Q., Wang, Z., Poon, S.C.N., Dube, W.P., Blake, D.R., Louie, P.K.K.,
4 Luk, C.W.Y., Tsui, W., Brown, S.S.: Observations of nitryl chlorine and modeling its source and effect on ozone
5 in the planetary boundary layer of southern China. *J. Geophys. Res.* 121, 2476e2489, 2016
- 6 Wang, H., Chen, J. and Lu, K.: Development of a portable cavity-enhanced absorption spectrometer for the
7 measurement of ambient NO₃ and N₂O₅: experimental setup, lab characterizations, and field applications in a
8 polluted urban environment, *Atmos. Chem. Phys.* 10, 1465-1479, 2017.
- 9 Wang, X., Wang, H., Xue, L., Wang, T., Wang, L., Gu, R., Wang, W., Than, Y. T., Wang, Z., Yang, L., Chen, J.
10 and Wang, W.: Observations of N₂O₅ and ClNO₂ at a polluted urban surface site in North China: High N₂O₅
11 uptake coefficients and low ClNO₂ product yields, *Atmos. Environ.*, 156, 125-134, 2017.
- 12 Wang, Z., Wang, W., Tham, Y. J., Hao, Q. L., Wang, L. W., Xinfeng., W., Wang, L. W. and Wang, T.: Fast
13 heterogeneous N₂O₅ uptake and ClNO₂ production in power plant plumes observed in the nocturnal residual layer
14 over the North China Plain, *Atmos. Chem. Phys. Discuss.*, 2017.
- 15 Wang, D. and Ruiz, L. H.: Secondary organic aerosol from chlorine-initiated oxidation of isoprene, *Atmos. Chem.*
16 *Phys. Discuss.*, 2017-342, 2017.
- 17 Whalley, L. K., Furneaux, K. L., Goddard, A., Lee, J. D., Mahajan, A., Oetjen, H., Read, K. A., Kaaden, N.,
18 Carpenter, L. J., Lewis, A. C., Plane, J. M. C., Saltzman, E. S., Wiedensohler, A., and Heard, D. E.: The chemistry
19 of OH and HO₂ radicals in the boundary layer over the tropical Atlantic Ocean, *Atmos. Chem. Phys.*, 10, 1555-
20 1576, <https://doi.org/10.5194/acp-10-1555-2010>, 2010.
- 21 Ye, Y., Galbally, I. E., Weeks, I. A., Duffy, B. L., and Nelson, P. F.: Evaporative emissions of 1,3-butadiene from
22 petrol-fuelled motor vehicles, *Atmos. Environ.*, 32, 2685-2692, 1998.
- 23 Simpson, D., Benedictow, A., Berge, H., Bergström, R., Emberson, L. D., Fagerli, H., Flechard, C. R., Hayman,
24 G. D., Gauss, M., Jonson, J. E., Jenkin, M. E., Nyíri, A., Richter, C., Semeena, V. S., Tsyro, S., Tuovinen, J.-P.,
25 Valdebenito, Á., and Wind, P.: The EMEP MSC-W chemical transport model – technical description, *Atmos.*
26 *Chem. Phys.*, 12, 7825-7865, <https://doi.org/10.5194/acp-12-7825-2012>, 2012.
- 27 Skamarock, W. C., J. B. Klemp, J. Dudhia, D. O. Gill, D. M. Barker, M. G Duda, X.-Y. Huang, W. Wang, and J.
28 G. Powers, 2008: A Description of the Advanced Research WRF Version 3. NCAR-Tech, 113,
29 doi:10.5065/D68S4MVH
- 30 Wiedinmyer, C., S. K. Akagi, R. J. Yokelson, L. K. Emmons, J. A. Al-Saadi, J. J. Orlando, and A. J. Soja. "The
31 Fire Inventory from Near (Finn): A High Resolution Global Model to Estimate the Emissions from Open Burning."
32 *Geoscientific Model Development* 4, no. 3 (2011): 625-41.
- 33 Kaiser, J. W., Heil, A., Andreae, M. O., Benedetti, A., Chubarova, N., Jones, L., Morcrette, J.-J., Razinger, M.,
34 Schultz, M. G., Suttie, M., and van der Werf, G. R. (2012). Biomass burning emissions estimated with a global
35 fire assimilation system based on observed fire radiative power. *Biogeosciences*, 9:527-554.

36

37

38

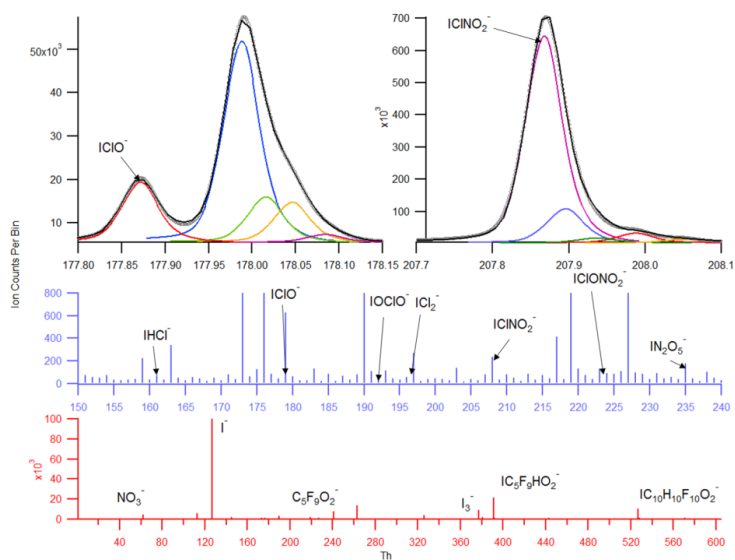


1 **Table 1. Identified Cl-VOC reaction products, nomenclature of Cl-VOC and precursor compound.**

Cl-VOC	Potential nomenclature	Precursor
CHClO	formyl chloride	formaldehyde
C ₂ H ₃ ClO	chloroacetaldehyde	acetaldehyde
C ₃ H ₅ ClNO ₅	Chloro PPN	PPN
C ₂ H ₃ ClNO ₅	chloro PAN	PAN
C ₃ H ₅ ClO	chloroacetone	acetone
C ₂ H ₃ ClO ₂	chloroacetic acid	acetic acid
CHClO ₂	chloroformic acid	formic acid
C ₄ H ₇ ClO	chloro MEK or butanal	isoprene
C ₅ H ₆ ClO	CMBO - chloro 3-methyl-3-butene-2-one	isoprene
C ₅ H ₉ ClO ₂	-	isoprene
C ₅ H ₉ ClO ₃	-	isoprene
C ₃ H ₅ ClO	propanoyl chloride	1, 3 butadiene
C ₈ H ₉ Cl	chloroethyl benzene	aromatic

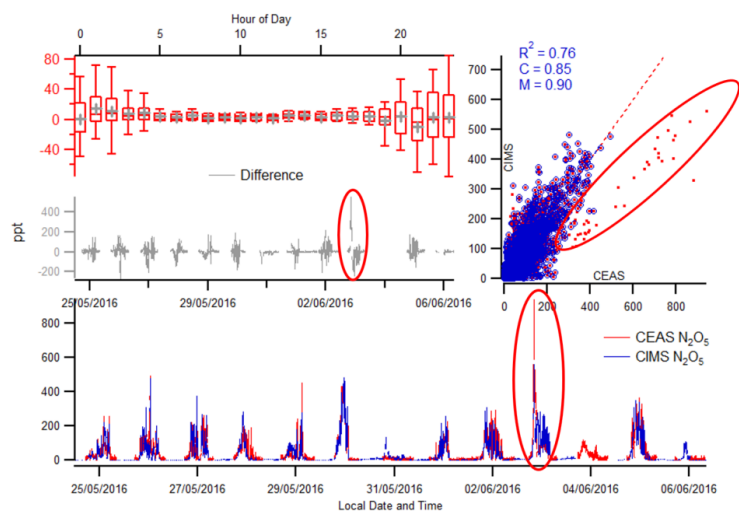
2

3



4

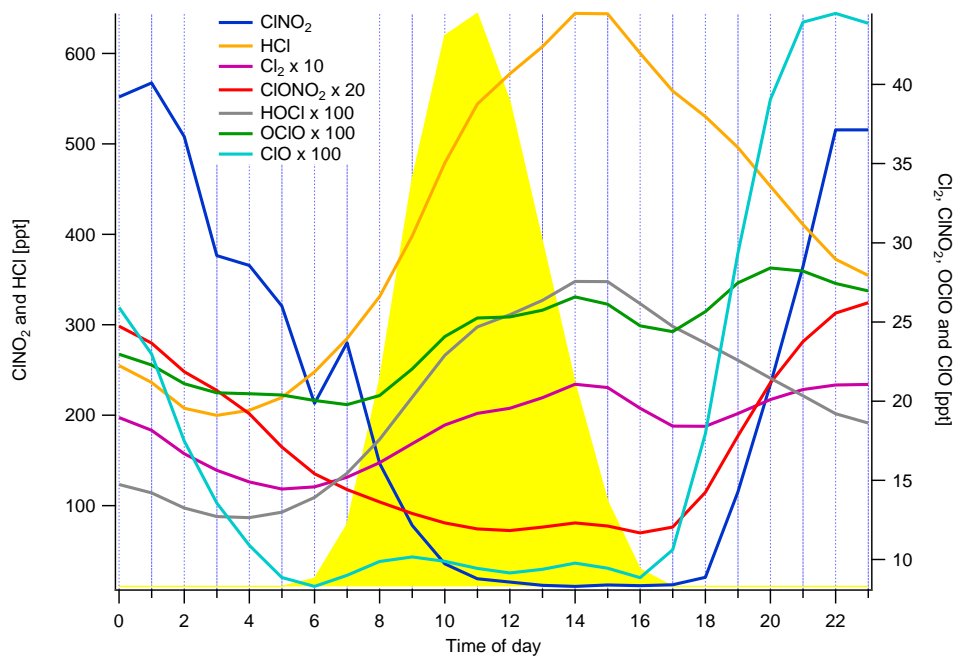
5 **Figure 1. Average high resolution mass spectrum for the whole measured range (red) and for the region**
 6 **that contains all gas phase night time species utilised in this work (blue). A high resolution spectral fit for**
 7 **ClO and ClNO₂ are displayed with corresponding multi peaks with 0.5 AMU. The black line represents the**
 8 **total fit from all peaks. The grey line represents the mass spectral raw data.**



1

2 **Figure 2. CIMS and CEAS one minute averaged data of N_2O_5 with corresponding correlation plot,**
3 **campaign and diurnal deviation. The red highlighted periods represent data collected on the 3rd June where**
4 **a different correlation gradient was observed between CIMS and CEAS. The box and whisker plot**
5 **represents the diurnal difference for the campaign between the CEAS and CIMS measurements.**

6

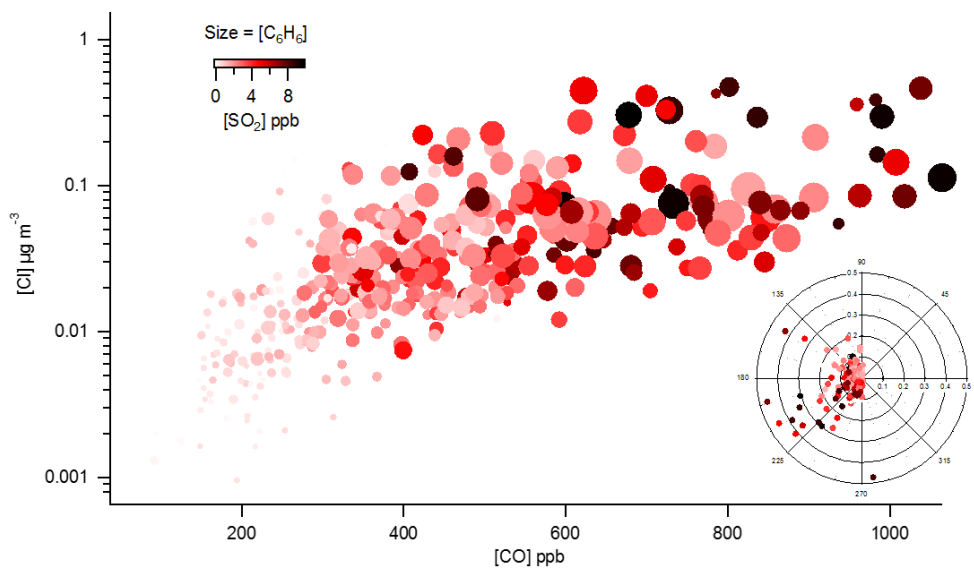


7



- 1 **Figure 3. Mean diurnal profiles of the inorganic halogens detected by the CIMS from the 23rd May to 6th**
2 **June with average J rate for ClNO₂ as guide for photolysis. ClNO₂ and HCl concentrations are on the left**
3 **y-axis and the other inorganic halogens on the right y-axis**

4



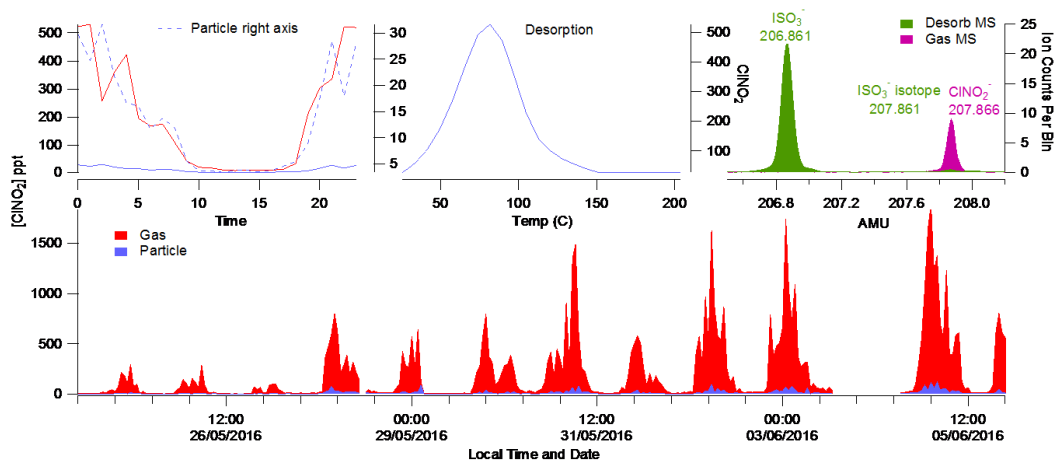
5

- 6 **Figure 4. Correlation of particulate Cl⁻ from the AMS measurements and CO colour coded by SO₂**
7 **concentration and size binned by increasing benzene concentration. A wind rose plot illustrates the wind**
8 **direction and particulate Cl⁻ concentration colour coded by SO₂ concentration.**

9

10

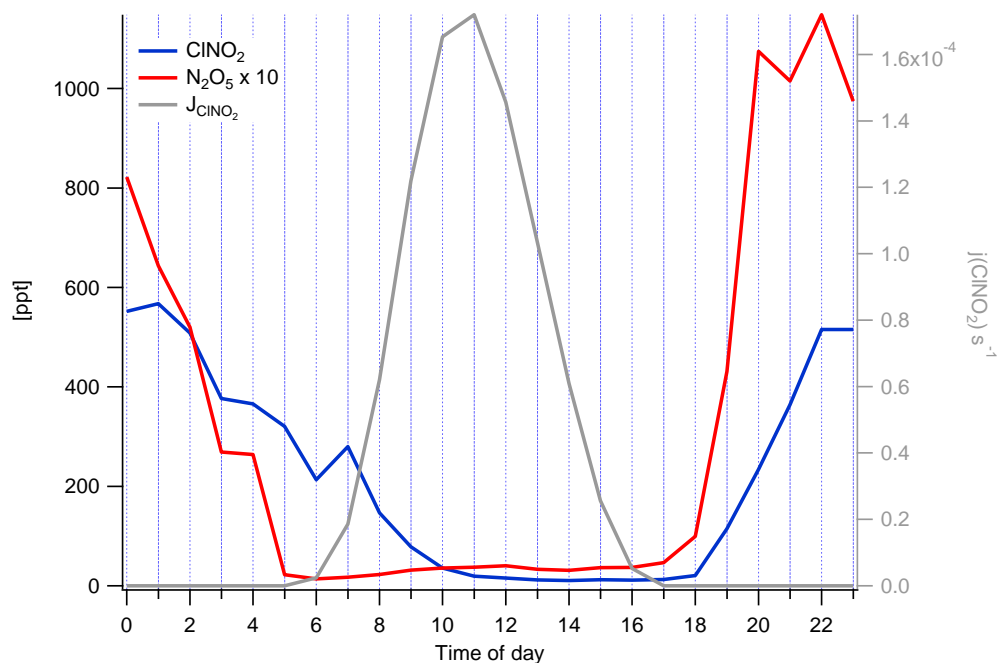
11



1

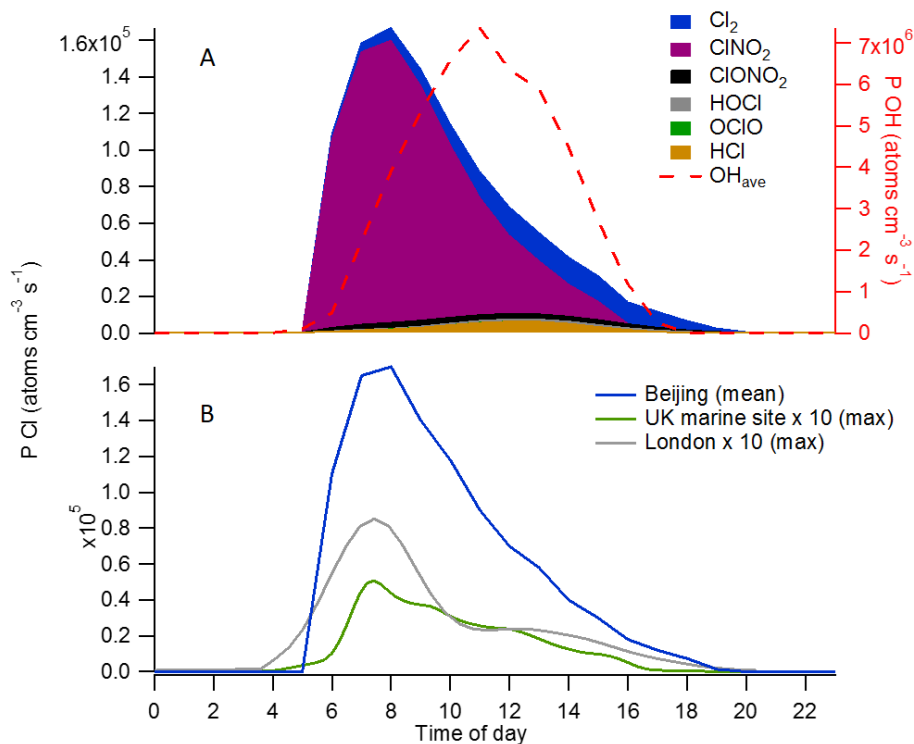
2 **Figure 5.** CINO₂ gas and particle phase campaign time series (1 hour averaged) and average diurnal profiles.
3 **The peak fitting for CINO₂ and the SO₃ interfering mass at 207-208 AMU is shown and the desorption**
4 **profile for the counts attributed to the high resolution CINO₂ peak.**

5



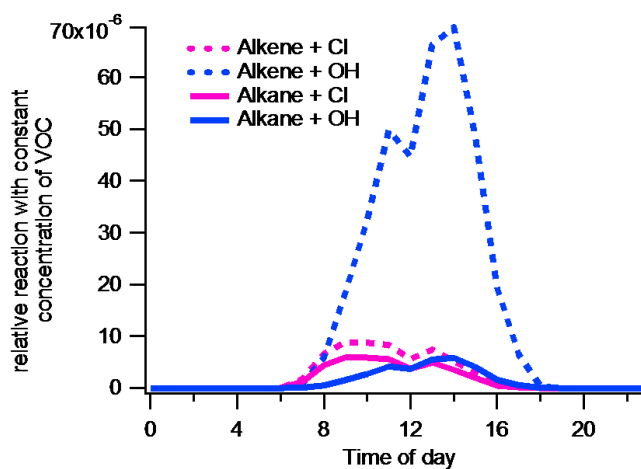
6

7 **Figure 6.** Diurnal profile of N₂O₅, CINO₂ and j(CINO₂) for the campaign highlighting the persistence of
8 CINO₂ passed sunrise and the expected rapid photolysis of N₂O₅.



1

2 **Figure 7. A) Contribution of inorganic halogens to chlorine atom production. B) Relative mean diurnal**
3 **profiles of calculated chlorine atom concentrations from this work (Beijing) and measurements in the UK**
4 **(London (Bannan et al., 2015) and a marine site (Weybourne Atmospheric Observatory-Bannan et al.,**
5 **(2017)). The steady state OH production rate from Beijing is also displayed to illustrate relative**
6 **concentrations of oxidants.**

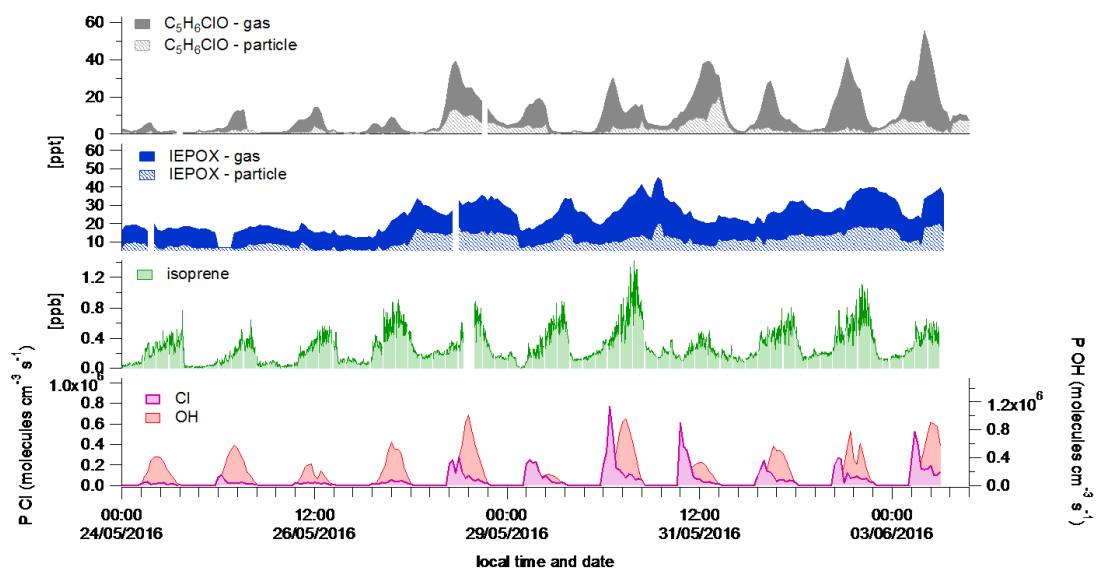


7



1 **Figure 8. Mean diurnal time series of alkene (pink) and alkane (blue) relative reaction rate (arbitrary value)**
2 **with the chlorine atom (dashed) and OH (solid).**

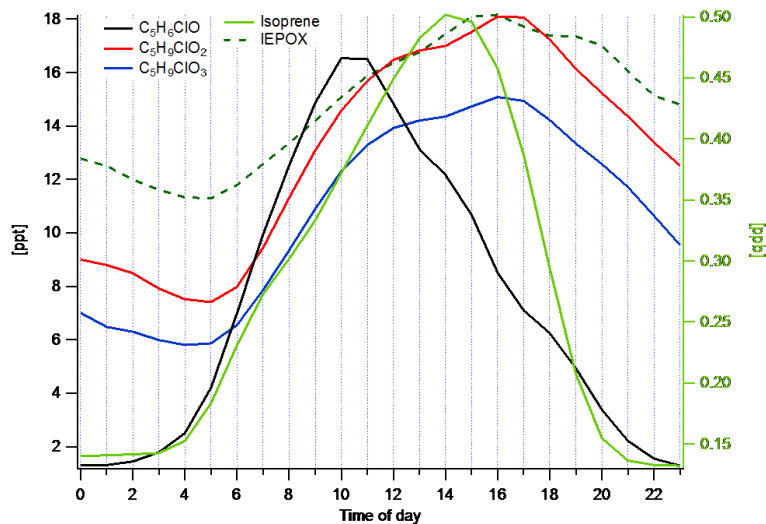
3



4

5 **Figure 9. Campaign time series of isoprene, IEPOX, CMBO and steady state production rate of chlorine**
6 **atoms and OH**

7

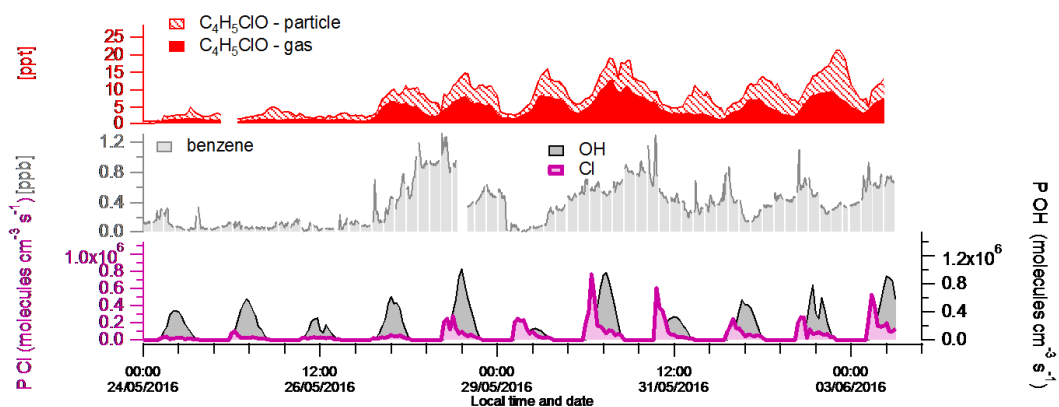


8



1 **Figure 10.** Mean diurnal profiles of isoprene (right y-axis) and its OH oxidation product (IEPOX) and
2 chlorine atom oxidation products CMBO, $C_5H_9ClO_2$ and $C_5H_9ClO_3$ (left y-axis)

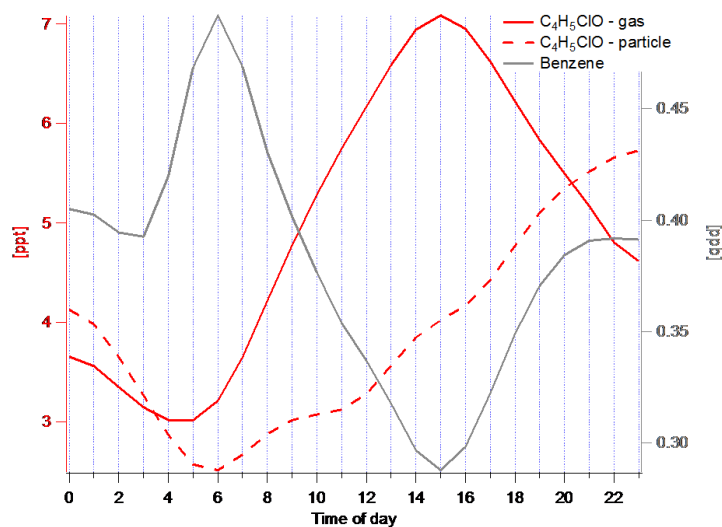
3



4

5 **Figure 11.** Campaign time series of benzene and CCA with supporting calculations of OH and the chlorine
6 atom production rates

7



8

9 **Figure 12.** Mean campaign diurnal profiles of benzene (grey) and CCA in the particle (dashed red) and gas
10 phase (solid red).

11